

Electronic Supplementary Information (ESI):

Statistical copolymer metal organic nanotubes

Jacob A. Barrett,^a Nathan D. Rosenmann,^b Karthikeyan Gnanasekaran,^b Xian B. Carroll,^a Nathan C. Gianneschi,^{*b} and David M. Jenkins^{*a}

^a Department of Chemistry, University of Tennessee, Knoxville, Tennessee 37996, United States

^b Departments of Chemistry, Materials Science & Engineering, Biomedical Engineering, Pharmacology, International Institute for Nanotechnology, Simpson-Querrey Institute, Chemistry of Life Processes Institute, Lurie Cancer Center, Northwestern University, Evanston, Illinois, 60208, United States

Table of Contents

I.	Experimental Section	S2
II.	Single Crystal X-ray Structures	S7
III.	Selected Spectra and other Analytical Data	S10
IV.	Powder X-ray Diffraction Data	S19
V.	Selected Area Electron Diffraction	S21
VI.	STEM Imaging and Energy Dispersive X-Ray Spectroscopy	S23
VII.	References	S25

I. Experimental Section

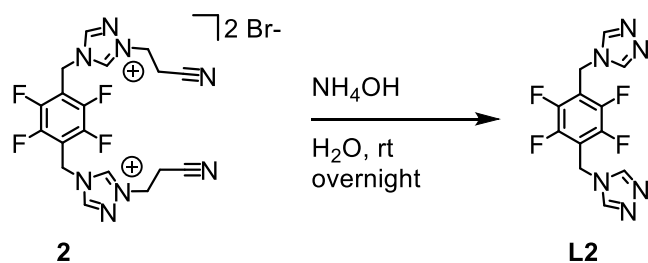
General Considerations for Synthesis

The compounds 1,2,4-triazole-1-propanenitrile,¹ 4,4'-(1,4-(xylene)diyl)bis-1-(2-cyanoethyl)-1,2,4-triazolium dibromide,² 4,4'-(1,4-(xylene)diyl)bis(1,2,4-triazole) (**L1**),² and [(**L1**)Cu₂Br₂] • DMF² were prepared as previously described. Solvents used under N₂ atmosphere were purchased anhydrous (methanol) or dried with an Innovative Technologies (Newburyport, MA) Pure Solv MD-7 Solvent Purification System, degassed by three freeze-pump-thaw cycles, and stored over 4 Å molecular sieves (dichloromethane). All other reagents and solvents were purchased from commercial vendors and used without further purification.

¹H and ¹⁹F{¹H} NMR spectra were recorded in dimethylsulfoxide-d₆ at 25 °C on a Bruker AVANCE NEO 500 MHz system. Solution-state ¹³C{¹H} and ¹⁹F{¹³C} NMR spectra were recorded in dimethylsulfoxide-d₆ at ambient temperature on a Varian VNMRS 500 MHz system. Solid-state ¹³C{¹H} CP-MAS spectra were recorded on a Varian INOVA 400 MHz system. ¹H and ¹³C chemical shifts were referenced to the residual NMR solvent in the solution state³ or externally to adamantane in the solid state,⁴ while ¹⁹F chemical shifts were externally referenced to trifluoroacetic acid in DMSO-d₆.⁵ All mass spectrometry analyses were conducted at the Biological and Mass Spectrometry Core Facility located in the Department of Chemistry at the University of Tennessee. DART analyses were performed using a JEOL AccuTOF-D time-of-flight (TOF) mass spectrometer with a DART (direct analysis in real time) ionization source from JEOL USA, Inc. (Peabody, MA). ESI/MS analysis was performed using a QSTAR Elite quadrupole time-of-flight (QTOF) mass spectrometer with an electrospray ionization source from AB Sciex (Concord, Ontario, Canada). Infrared spectra were collected neat on a Thermo Scientific Nicolet iS10 with a Smart iTR accessory for attenuated total reflectance. Thermogravimetric analysis was collected on freshly prepared samples on a TA Instruments TGA Q50 under N₂. Gas adsorption measurements were collected on a Micromeritics ASAP 2020. Carbon, hydrogen, and nitrogen analyses were obtained from Galbraith Laboratories Inc., Knoxville, TN.

MHz): δ 10.48 (s, 2H), 9.46 (s, 2H), 5.84 (s, 4H), 4.73 (t, $J = 6.3$ Hz, 4H), 3.25 (t, $J = 6.3$ Hz, 4H). $^{13}\text{C}\{^1\text{H}\}$ NMR (DMSO- d_6 , 125.79 MHz): δ 145.06, 143.94, 117.59, 47.27, 38.94, 17.22 [Note: Carbons on aryl ring are not observed due to ^{19}F splitting.]. $^{13}\text{C}\{^{19}\text{F}\}$ NMR (DMSO- d_6 , 125.79 MHz): δ 145.04 (d, $J = 261$ Hz), **144.15** (s), 143.99 (d, $J = 229$ Hz), 117.66 (s), **113.36** (s), 47.31 (t, $J = 150$ Hz), 39.05 (t, $J = 304$ Hz), 17.26 (t, $J = 140$ Hz) [Note: **Bold** numbers are resonances for carbons on aryl ring.]. $^{19}\text{F}\{^1\text{H}\}$ NMR (DMSO- d_6 , 470.62 MHz): δ -140.21. IR(neat): 3026, 3005, 2986, 2941, 2256, 1824, 1575, 1523, 1498, 1455, 1408, 1387, 1357, 1335, 1289, 1275, 1236, 1191, 1154, 1072, 1048, 1011, 989, 949, 923, 870, 824, 777, 683, 657, 635 cm^{-1} . HR ESI-MS (m/z): $[\text{M}-2\text{Br}]^{2+}$ 210.0719 (found), $\text{C}_{18}\text{H}_{16}\text{F}_4\text{N}_8^{2+}$: 210.0717 (calcd).

Synthesis of 4,4'-(1,3-(2,3,5,6-tetrafluoroxylene)diyl)bis(1,2,4-triazole), L2.



4,4'-[1,4-(2,3,5,6-tetrafluoroxylene)diyl]bis-(1-(2-cyanoethyl)-1,2,4-triazolium) dibromide (22.4 g, 38.5 mmol) was dissolved in 175 mL saturated ammonium hydroxide solution and the solution was stirred at room temperature overnight. The resulting white precipitate was filtered off, and the mother liquor was retained for an additional two days for further precipitation. Precipitates were combined, rinsed with H_2O (2x40 mL), rinsed with diethyl ether (2x5 mL) and dried under reduced pressure to yield an off-white powder (9.13 g, 75.9% yield) as a white powder. ^1H NMR (DMSO- d_6 , 500.21 MHz): δ 8.58 (s, 4H), 5.49 (s, 4H). $^{13}\text{C}\{^1\text{H}\}$ NMR (DMSO- d_6 , 125.79 MHz): δ 144.43 (dm, $J = 252$ Hz), 143.22 (s), 115.12 (m), 35.78 (t, $J = 2.4$ Hz). $^{13}\text{C}\{^{19}\text{F}\}$ NMR (DMSO- d_6 , 125.79 MHz): δ 144.46 (t, $J = 4.5$ Hz), 143.26 (dq, $J_A = 211$ Hz, $J_B = 3.1$ Hz), 115.12 (t, $J = 5.0$ Hz), 35.81 (t, $J = 147$ Hz). $^{19}\text{F}\{^1\text{H}\}$ NMR (DMSO- d_6 , 470.62 MHz): δ -142.48. IR(neat): 3098, 2966, 1672, 1532, 1519, 1490, 1459, 1424, 1382, 1361, 1347, 1335, 1286, 1225, 1184, 1074, 1066, 1046, 1028, 1014, 976, 968, 948, 877, 865, 838, 771, 751, 679, 656 cm^{-1} . DART HR MS (m/z): $[\text{M}+\text{H}]^+$ 312.0835 (found); $\text{C}_{12}\text{H}_8\text{F}_4\text{N}_6$: 312.0825 (calcd).

Synthesis of [(L₂)Cu₂Br₂] MONT.

Following previously published methods,² L₂ (157 mg, 0.503 mmol) was dissolved in 13.4 mL dimethylformamide in a 20 mL vial. Separately, CuBr₂ (225 mg, 1.01 mmol) was dissolved in 6.7 mL H₂O in a 4-dram vial. The solutions were heated to 85 °C in an aluminum heating block for 30 minutes, mixed, and heated without further agitation for an additional 14 d. Colorless needles were formed, and an aliquot was removed from the bulk product for XRD analysis. The remainder was isolated and washed with water and methanol (3 × 1 mL each), followed by Soxhlet extraction overnight with methanol and removal of residual solvent under reduced pressure to yield a white powder (297 mg, 98.7% yield). IR(neat): 3533, 3406, 3126, 2939, 2887, 2857, 1633, 1560, 1491, 1428, 1403, 1386, 1368, 1292, 1262, 1215, 1190, 1088, 1058, 1025, 952, 875, 799, 774, 695, 652 cm⁻¹. Anal. Calcd. for C₁₂H₈Br₂Cu₂F₄N₆: C, 24.05; H, 1.35; N, 14.03. Found: C, 23.88; H, 1.09; N, 13.93.

Synthesis of [(L₁)_x(L₂)_{1-x}Cu₂Br₂] MONTs.

14.0 mL dimethylformamide were added to each vial containing a mixture of ligands L₁ and L₂ (525 mM total) as follows:

	x = 0.8	x = 0.5	x = 0.2
mass L1 (mg)	101	63.1	25.3
mass L2 (mg)	32.8	81.9	131
reaction yield	310 mg, 84.2 %	310 mg, 81.7 %	329 mg, 84.1 %

Separately, 1.36 g CuBr₂ were dissolved in 40.1 mL H₂O (152 mM). The solutions were then heated to 85 °C in an aluminum heating block for 30 minutes. 7 mL of preheated CuBr₂ solution was pipetted into each ligand mixture, vials were then sealed, mixed on a vortex mixer for 2 minutes, and heating was resumed. After 14 days, colorless needles formed, were isolated, and washed with water and methanol (3 × 5 mL each). Solvent was removed under reduced pressure to yield white powders.

Anal. Calcd. for [(L₁)_{0.5}(L₂)_{0.5}Cu₂Br₂]: C₁₂H₁₀Br₂Cu₂F₂N₆: C, 25.59; H, 1.79; N, 14.93. Found: C, 26.41; H, 1.97; N, 14.95.

Post-synthetic mixing of MONTs [(L₁)Cu₂Br₂] and [(L₂)Cu₂Br₂]. Discrete [(L₁)Cu₂Br₂] and [(L₂)Cu₂Br₂] MONTs were synthesized as described. 11 mg [(L₁)Cu₂Br₂] MONT and 12 mg [(L₂)Cu₂Br₂] MONT were combined in a solution of 2 mL DMF and 1 mL H₂O, briefly mixed, then removed and dried for powder X-ray diffraction measurements.

X-ray Structure Determinations

Data were collected on a Bruker SMART APEXII diffractometer equipped with an APEXII CCD detector and operated at 1,800 W power (45 kV, 40 mA), employing the use of Mo K α radiation ($\lambda = 0.71073$ Å). The incident X-ray beam was focused and monochromated using Bruker Excalibur focusing optics.

Single crystals of ligand (**L2**, colorless needle) and MONT samples ($[(\mathbf{L1})_x(\mathbf{L2})_{1-x}\text{Cu}_2\text{Br}_2]$, all colorless needles) were mounted on nylon CryoLoops (Hampton Research) with Paratone-N (Hampton Research) and frozen at 100 K. Initial scans of each specimen were taken to obtain preliminary unit cell parameters and to assess the mosaicity (i.e. breadth of spots between frames) of the crystal to select the required frame width for data collection. In all cases, frame widths of 0.5° were judged to be appropriate and full hemispheres of data were collected using the Bruker APEX3 software suite to carry out overlapping φ and ω scans at a detector setting of $2\theta = 28^\circ$.

All data sets were reduced with Bruker SAINT and were corrected for absorption using SADABS. Structures were solved and refined using SHELXT and SHELXL-2018, respectively.

Powder X-ray Experiments

Powder X-ray diffraction data were collected on the samples using a Panalytical Empyrean θ - 2θ diffractometer in reflectance Bragg-Brentano geometry. Cu-K α radiation ($\lambda = 1.5406$ Å; 1,800 W, 45 kV, 40 mA) was focused using a planar Gobel Mirror riding the K α line. A 0.25 mm divergence slit was used for all measurements. Diffracted radiation was detected using a PIXcel3d detector [(6° 2θ sampling width) equipped with a Ni monochromator. Each sample was mounted onto a zero-background silicon plate fixed in a sample holder by placing the powdered sample directly onto the plate. The best counting statistics were achieved by using a 0.0394° 2θ step scan from $3 - 50^\circ$ with an exposure time of 118.30 s per step and a revolution spin rate of 4 s. Additional high-resolution scans were collected using a 0.0016° 2θ step scan from $14 - 20^\circ$ with an exposure time of 18.87 s per step and a revolution spin rate of 4 s.

Gas Adsorption Measurements

Gas adsorption measurements were performed on samples after PXRD analysis. All MONTs were activated prior to adsorption studies by solvent exchange with methanol as described in the previous section. All samples were degassed at 150°C for 24 h prior to measurements. CO $_2$ and CH $_4$ isotherms were collected at 298 K, while H $_2$ isotherms were collected at 77 K.

II. Single Crystal X-ray Structures

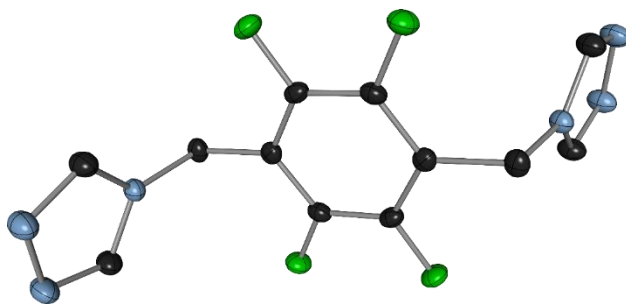


Figure S2. Single Crystal X-ray structure of **L2** ligand. Black, light blue, and green ellipsoids (50% probability) represent carbon, nitrogen, and fluorine atoms, respectively. Hydrogen atoms have been omitted for clarity.

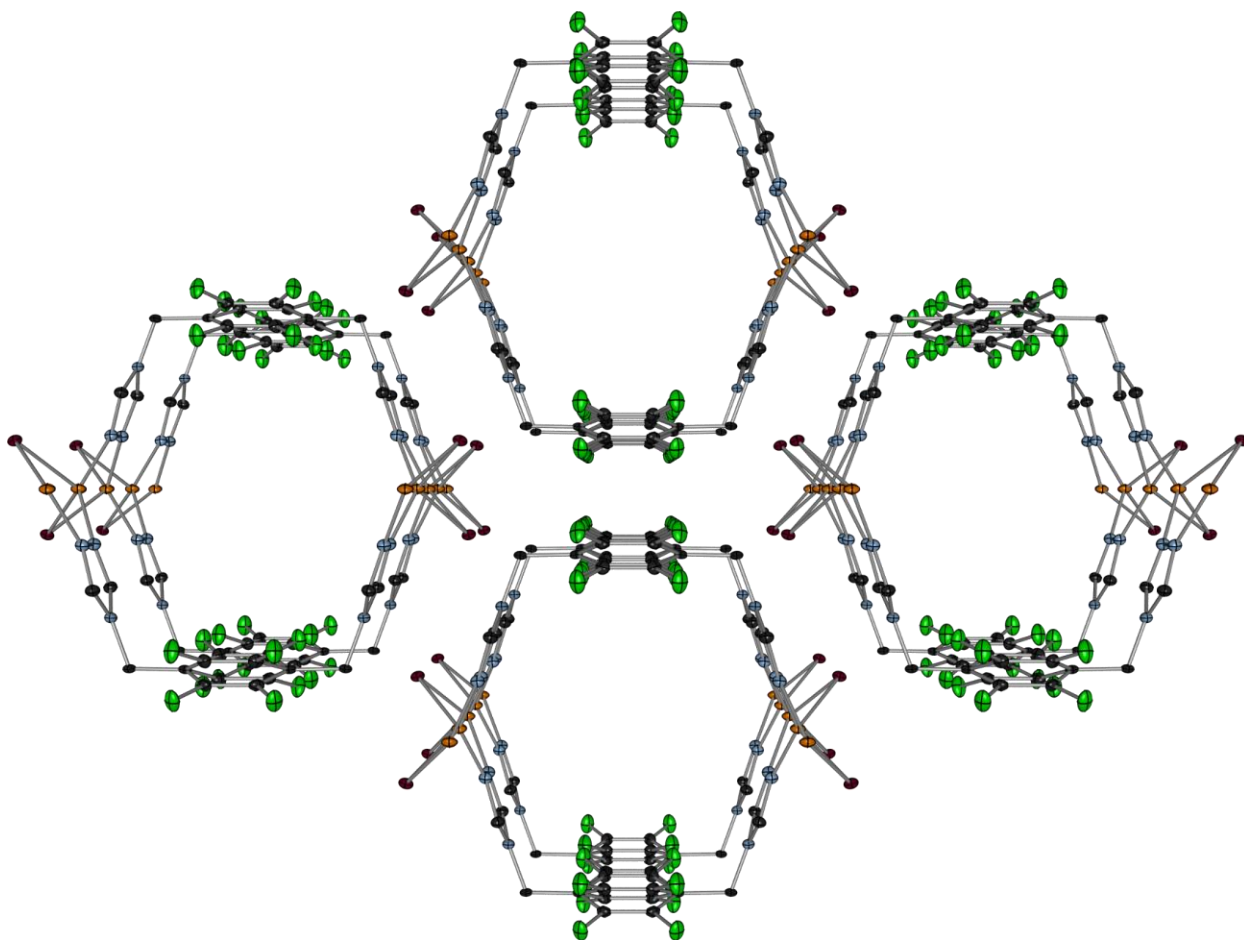
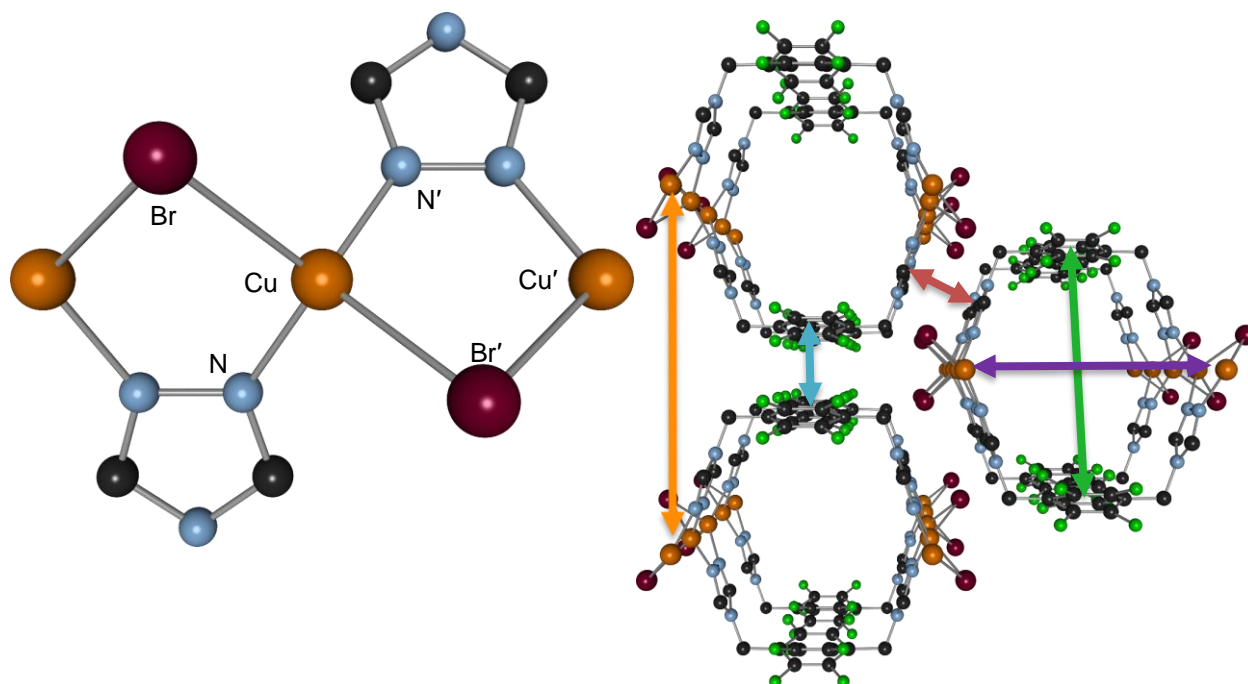


Figure S3. Single Crystal X-ray structure of $[(\mathbf{L2})\text{Cu}_2\text{Br}_2]$ MONT which shows tube packing. Black, light blue, green, orange, and purple ellipsoids (50% probability) represent carbon, nitrogen, fluorine, copper, and bromine atoms, respectively. Hydrogen atoms have been omitted for clarity.



	(L1)Cu ₂ Br ₂	(L1) _{0.8} (L2) _{0.2} Cu ₂ Br ₂	(L1) _{0.5} (L2) _{0.5} Cu ₂ Br ₂	(L1) _{0.2} (L2) _{0.8} Cu ₂ Br ₂	(L2)Cu ₂ Br ₂
Crystal system	Orthorhombic	Orthorhombic	Orthorhombic	Orthorhombic	Orthorhombic
Space group	Imma	Imma	Imma	Imma	Imma
a (Å)	20.611(7)	20.804(4)	20.9979(11)	21.1163(13)	21.2459(18)
b (Å)	7.029(2)	7.0172(9)	7.0308(4)	7.0507(4)	7.0831(6)
c (Å)	13.620(5)	13.5251(19)	13.4573(7)	13.4185(8)	13.3692(11)
α (°)	90	90	90	90	90
β (°)	90	90	90	90	90
γ (°)	90	90	90	90	90
Volume (Å ³)	1973.1(12)	1974.5(5)	1986.73(19)	1997.8(2)	2011.9(3)
Br–Cu (Å)	2.5990(8)	2.5837(5)	2.5759(2)	2.5741(4)	2.5691(2)
Cu–N (Å)	1.970(4)	1.969(3)	1.9739(14)	1.972(2)	1.9787(12)
Cu–Br–Cu'	85.08(4)	85.53(2)	86.059(10)	86.435(15)	87.145(11)
N–Cu–N'	140.3(2)	139.81(17)	140.22(8)	140.19(13)	140.33(7)
N–Cu–Br	102.01(10)	101.95(8)	101.77(4)	101.47(6)	101.03(3)
N–Cu–Br'	98.90(10)	98.99(8)	98.75(4)	98.92(6)	99.02(3)
Br–Cu–Br'	115.42(4)	116.15(3)	116.877(15)	117.37(2)	118.278(15)
Benzylc angle (°)	0.000(49)	0.000(40)	8.821(119)	12.252(92)	16.048(23)
Triazole distance (Å)	3.3499(314)	3.4145(55)	3.4560(27)	3.4692(37)	3.4775 (22)
Ring distance (Å)	3.6990(24)	3.5877(26)	3.5756(75)	3.5680(130)	3.5848(65)
Cu–Cu distance (Å)	13.6200(51)	13.5251(19)	13.4573(7)	13.4185(8)	13.3692(11)
pore width (Å)	9.2543(34)	9.2649(20)	9.3147(8)	9.3778(8)	9.4561(10)
pore height (Å)	9.9210(24)	9.9078(25)	9.8817(73)	9.8505(123)	9.7844(62)
Fluorine Occupancy	N/A	0.288	0.507	0.679	1

Table S1. Selected crystallographic data for [(L1)_x(L2)_{1-x}Cu₂Br₂] mixed ligand MONTs. [(L1)Cu₂Br₂] MONT data were previously published.²

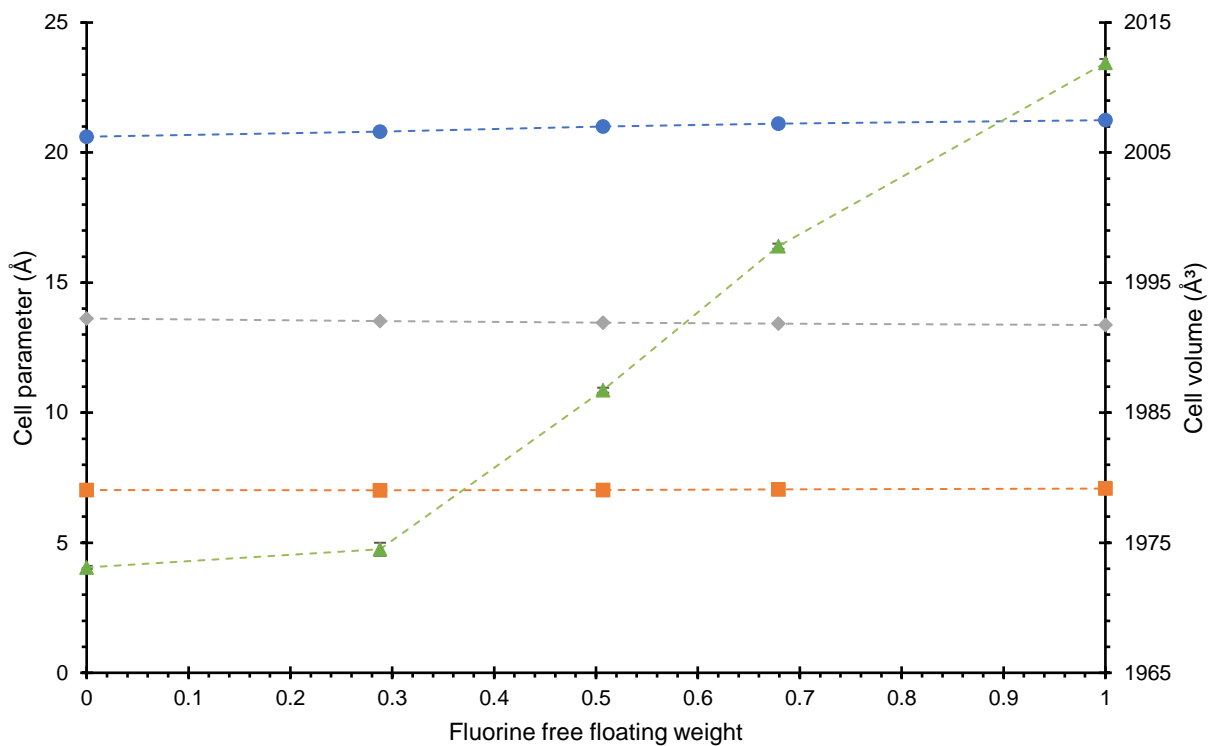


Figure S4. Crystallographic parameters as a function of fluorine occupancy (**Table S1**). a, b, and c cell parameters, as well as total cell volume, are represented by blue circles, orange squares, grey diamonds, and green triangles, respectively. Unit cell parameter error bars are obscured by data points.

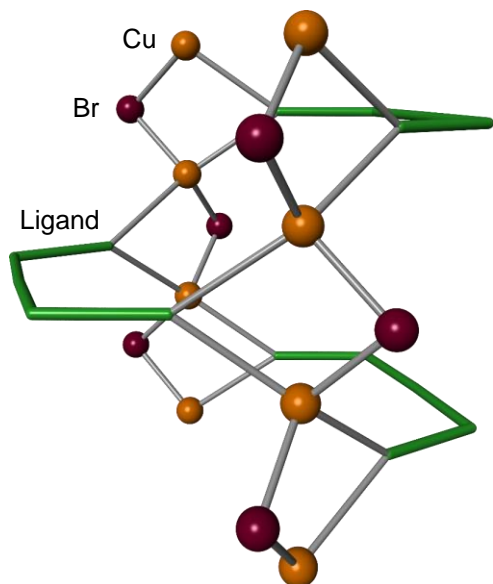


Figure S5. Representation of $[(L1)_x(L2)_{1-x}]Cu_2Br_2$ highlighting the (2,4) topology described in the manuscript. Linking organic ligands are represented by green rods, while copper and bromine atoms are represented by orange and purple spheres, respectively.

III. Selected Spectra and other Analytical Data

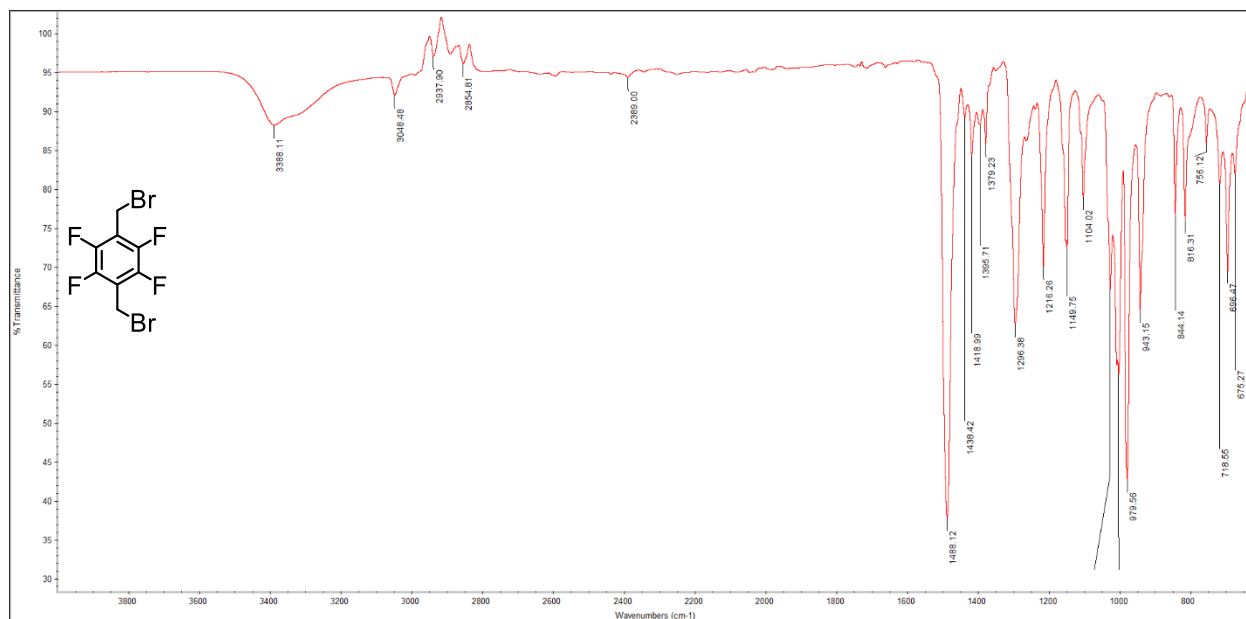


Figure S6. ATR-IR spectrum of **1**.

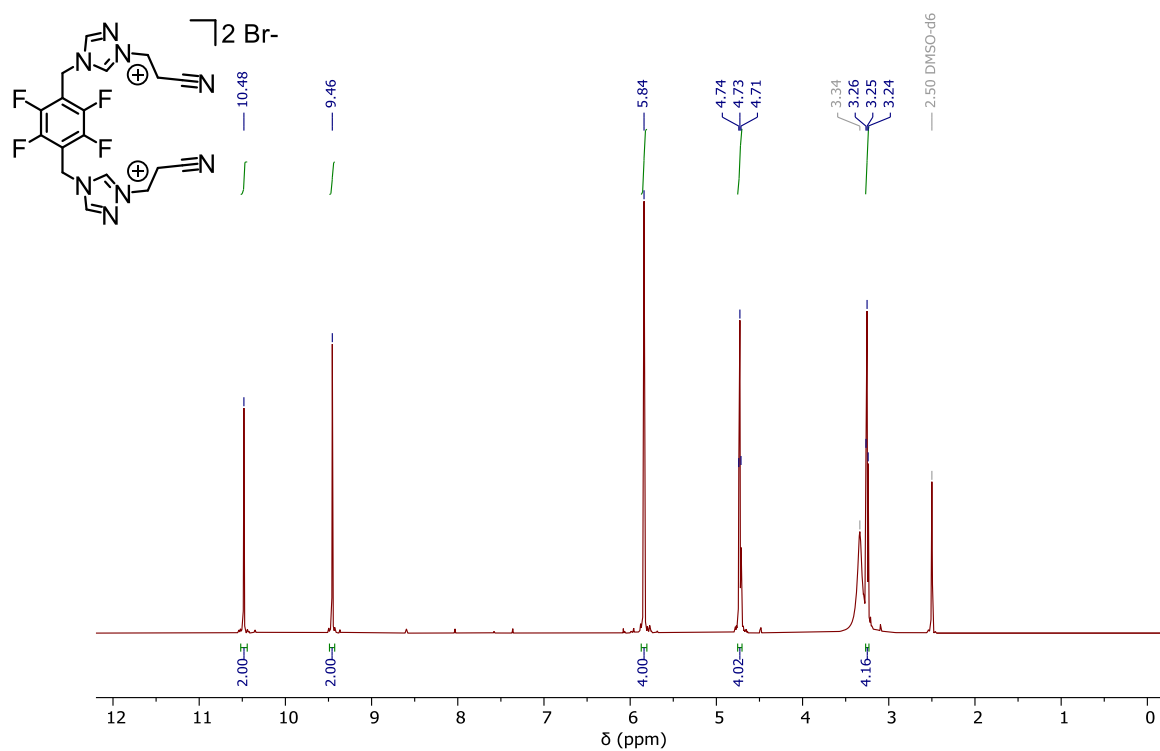


Figure S7. ¹H NMR spectrum of **2** in DMSO-*d*₆.

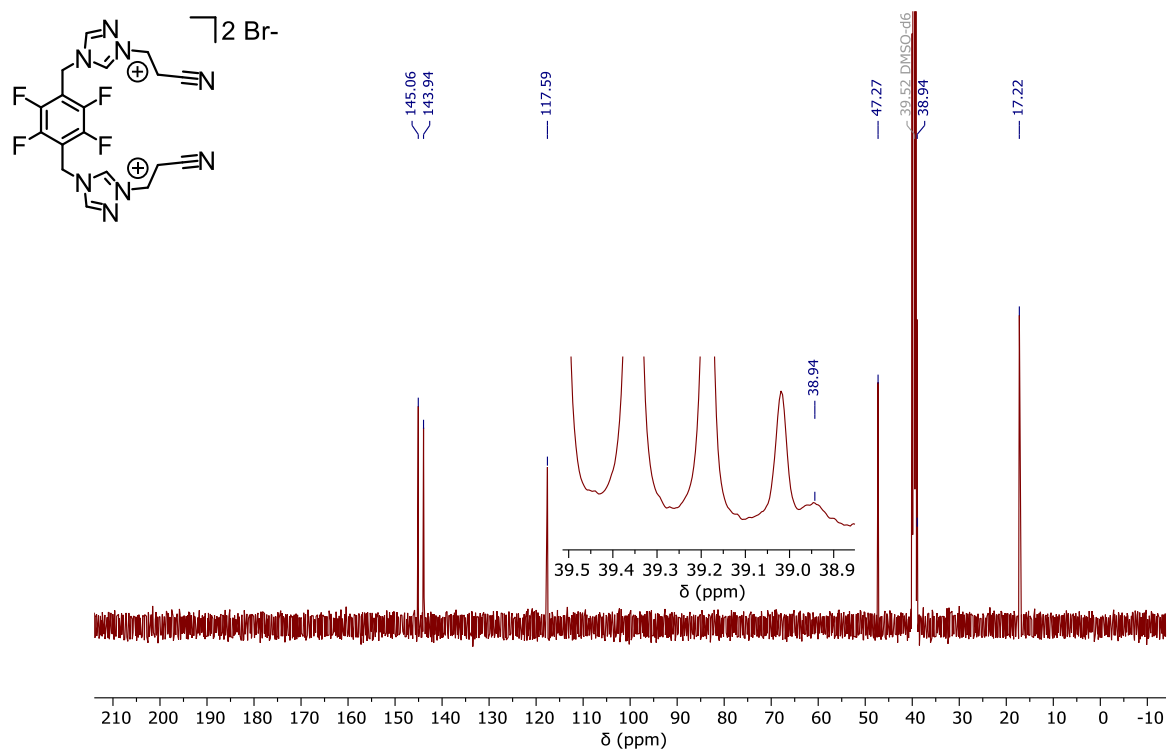


Figure S8. $^{13}\text{C}\{^1\text{H}\}$ NMR spectrum of **2** in $\text{DMSO-}d_6$.

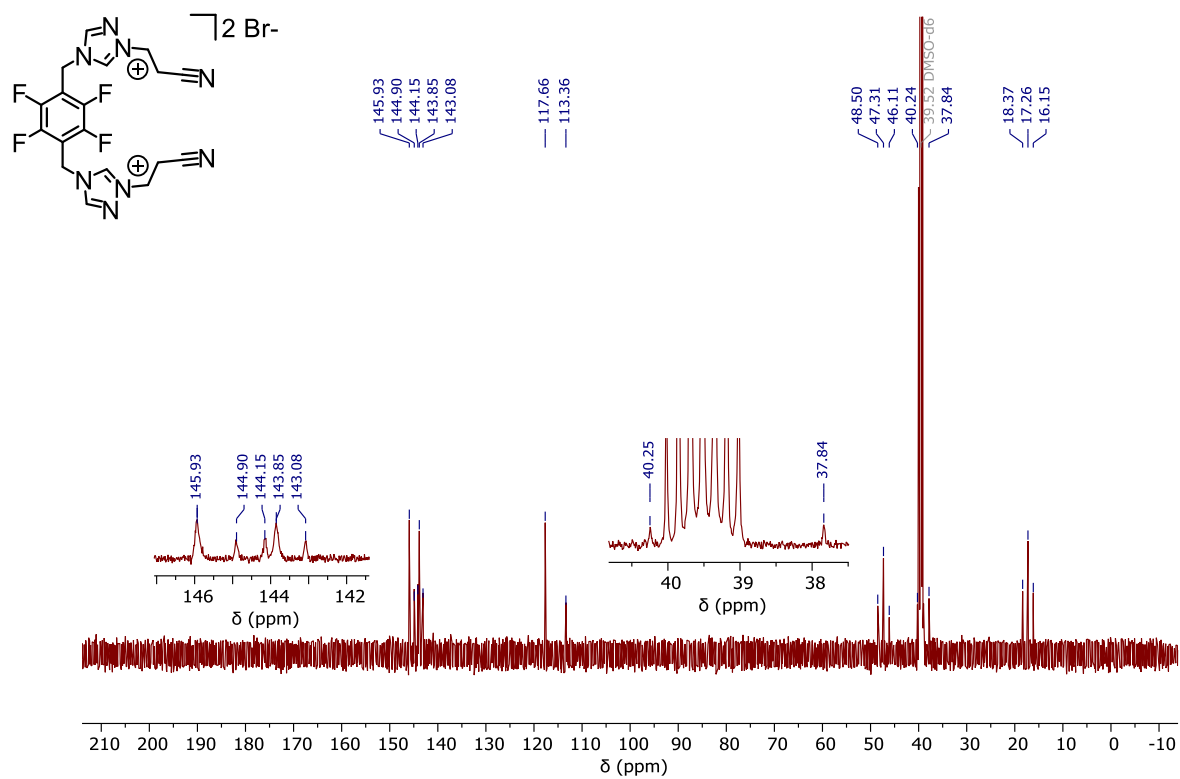


Figure S9. $^{13}\text{C}\{^{19}\text{F}\}$ NMR spectrum of **2** in $\text{DMSO-}d_6$.

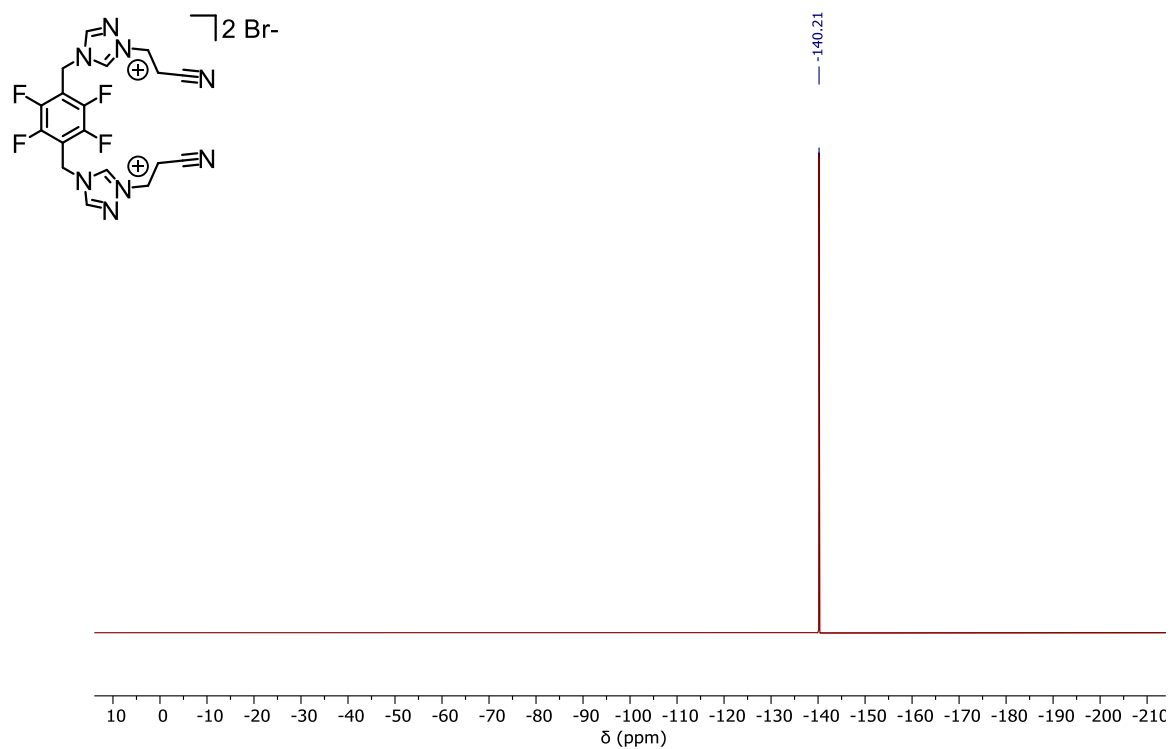


Figure S10. $^{19}\text{F}\{^1\text{H}\}$ NMR spectrum of **2** in $\text{DMSO-}d_6$.

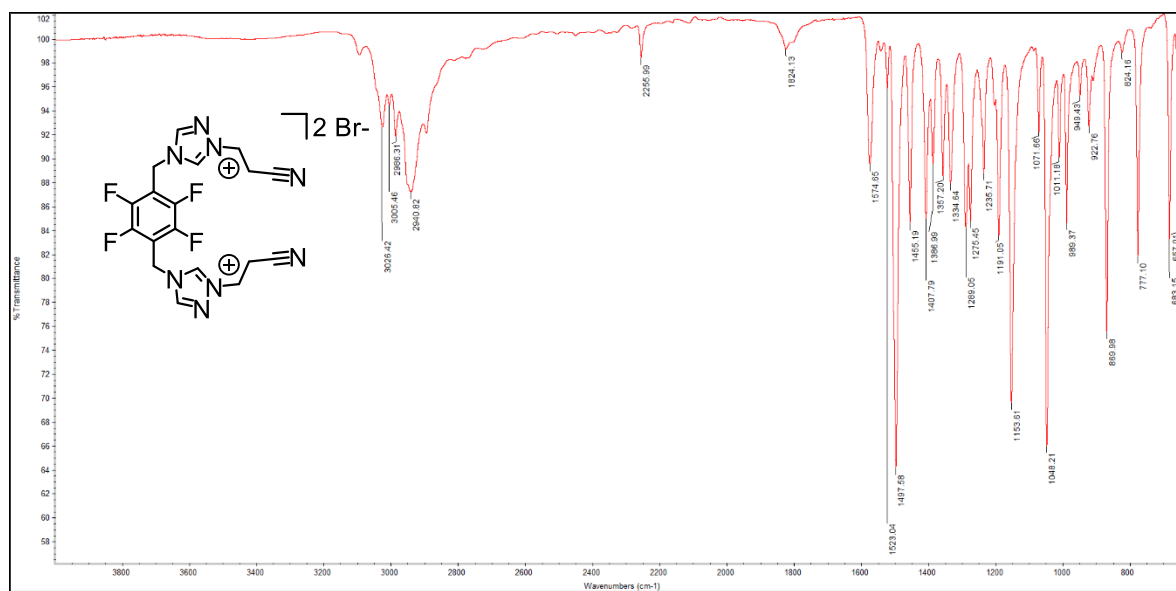


Figure S11. ATR-IR spectrum of **2**.

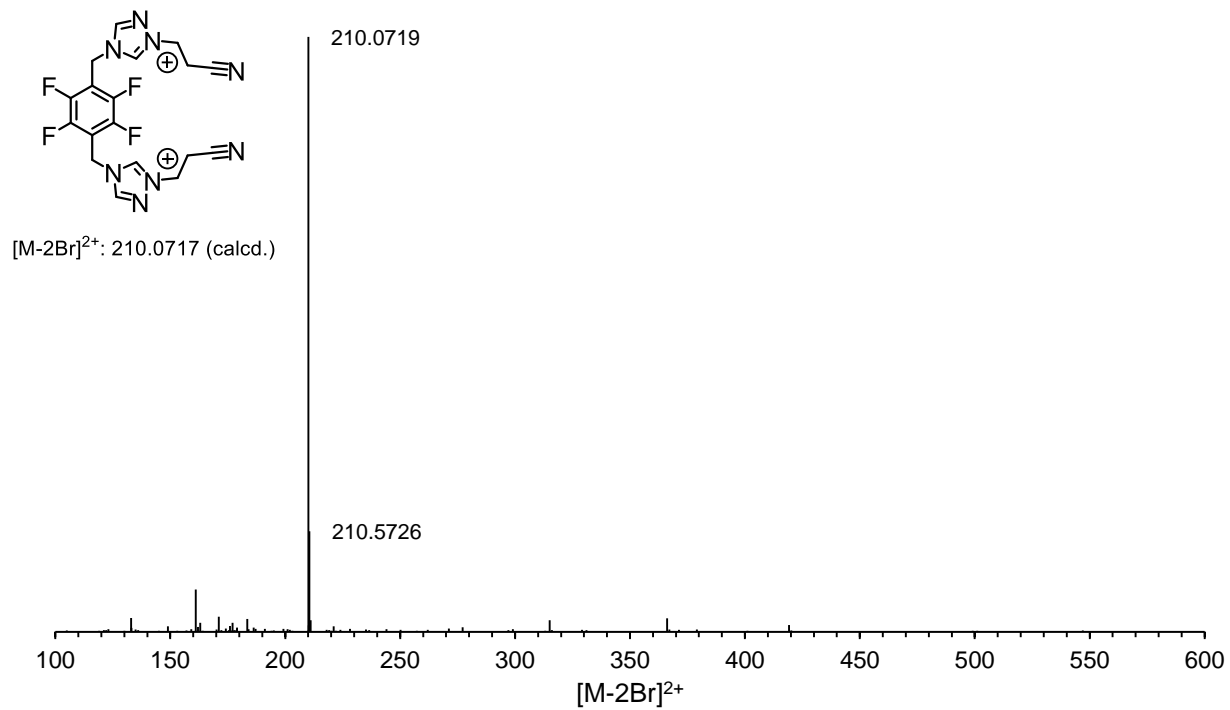


Figure S12. HR ESI-MS of **2**.

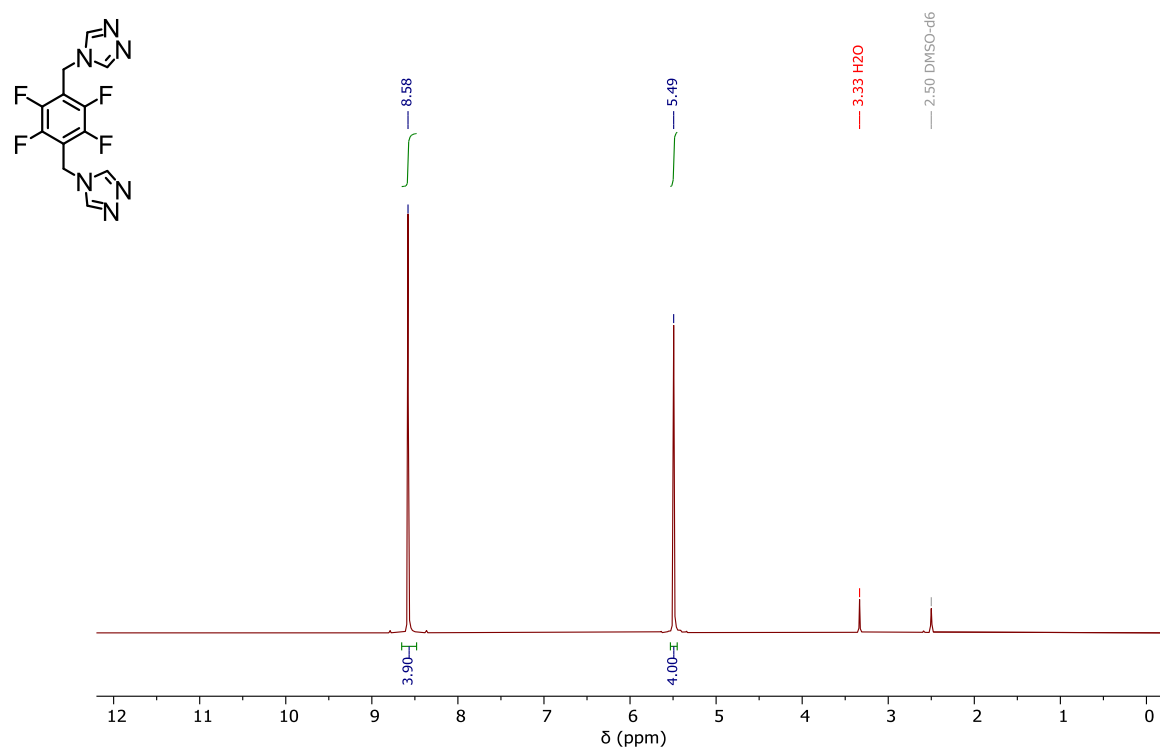


Figure S13. ^1H NMR spectrum of **L2** in DMSO-d_6 .

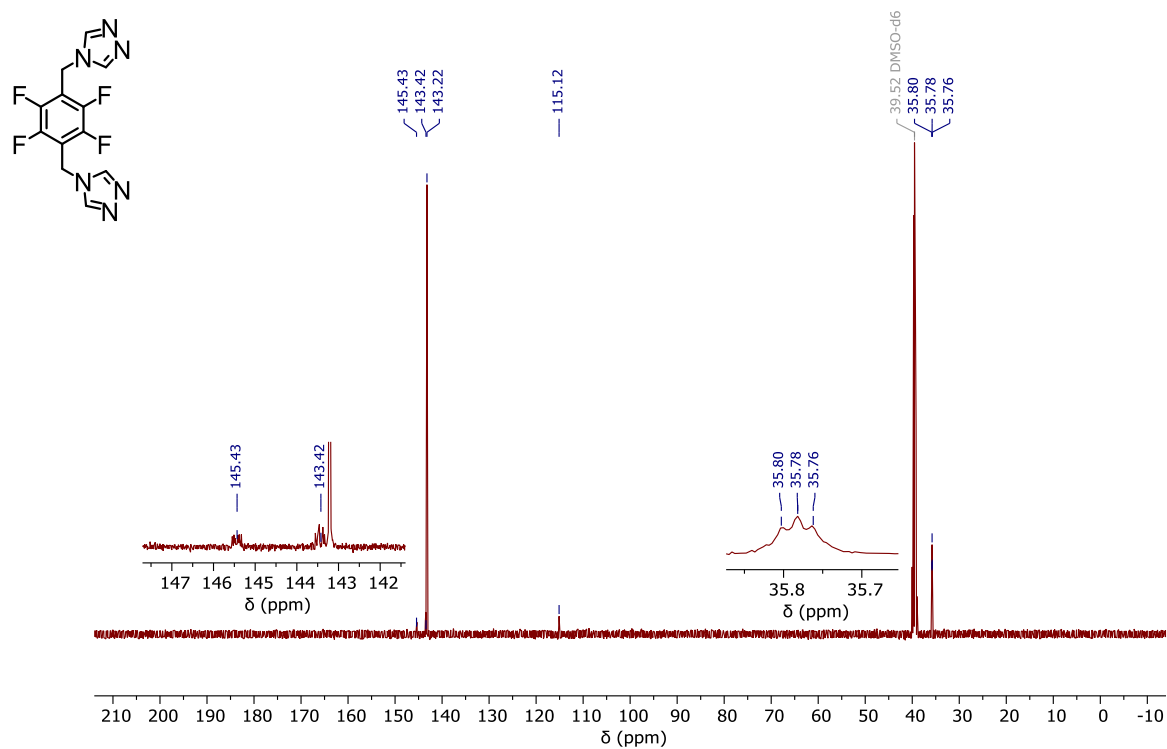


Figure S14. $^{13}\text{C}\{^1\text{H}\}$ NMR spectrum of L2 in DMSO- d_6 .

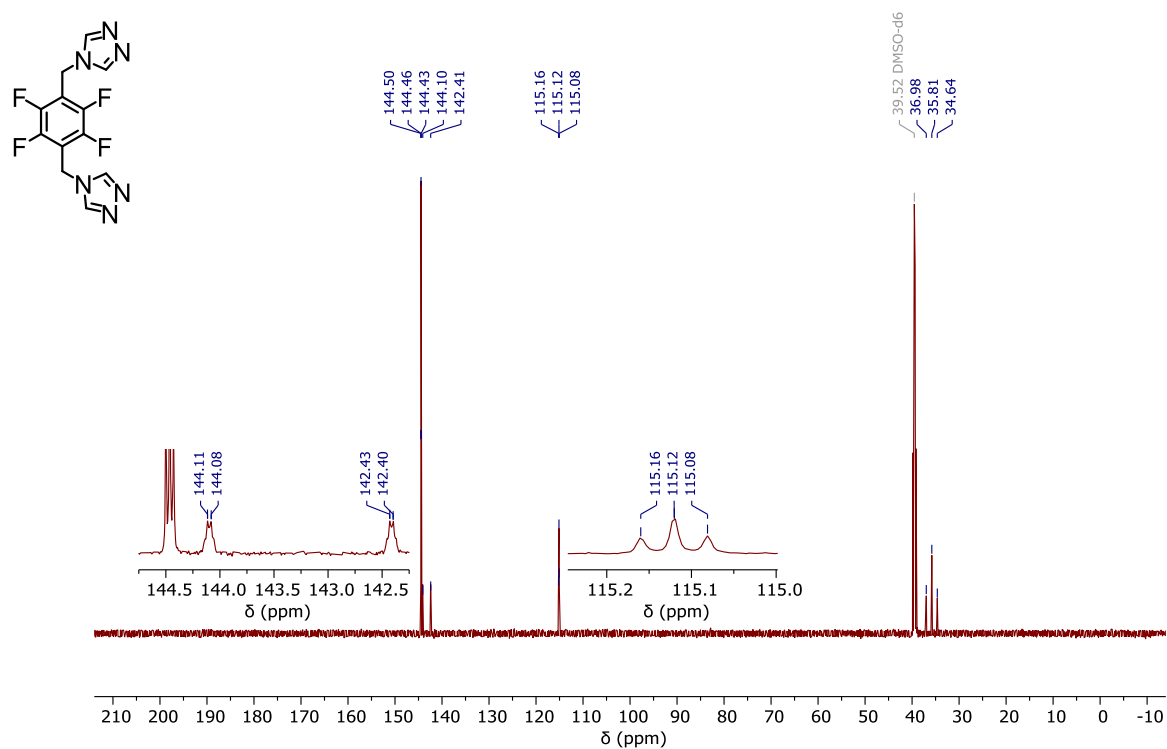


Figure S15. $^{13}\text{C}\{^{19}\text{F}\}$ NMR spectrum of L2 in DMSO- d_6 .

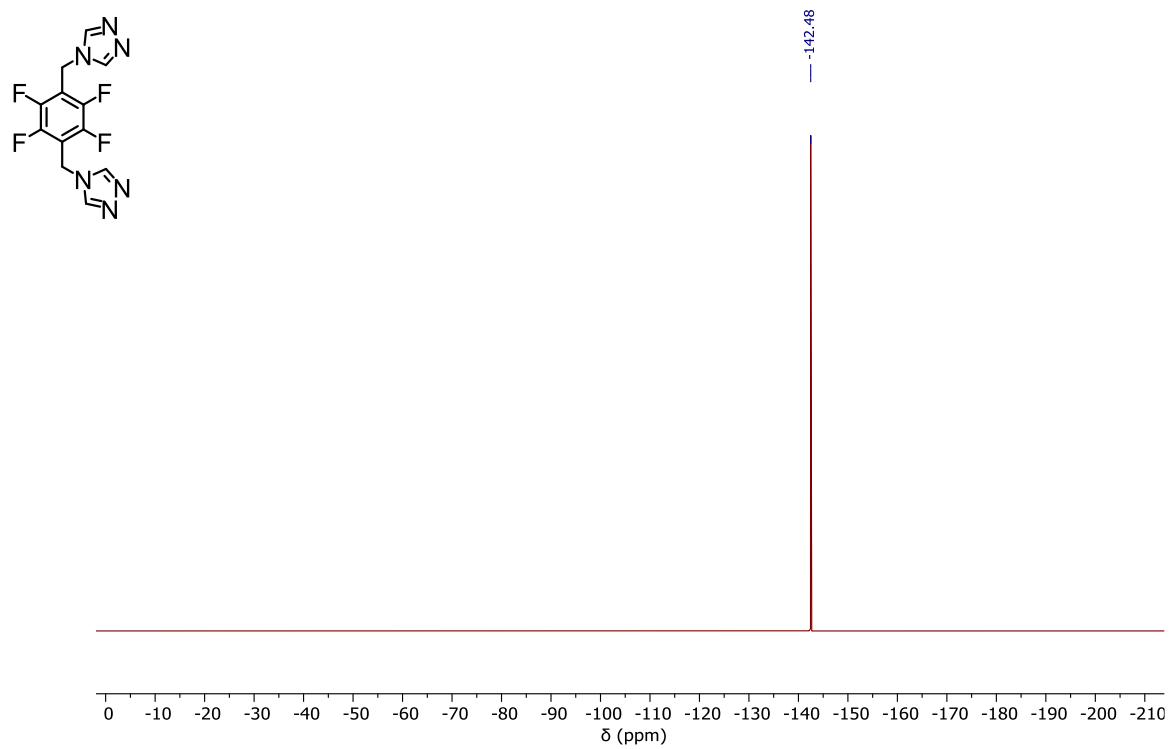


Figure S16. $^{19}\text{F}\{^1\text{H}\}$ NMR spectrum of L2 in DMSO- d_6 .

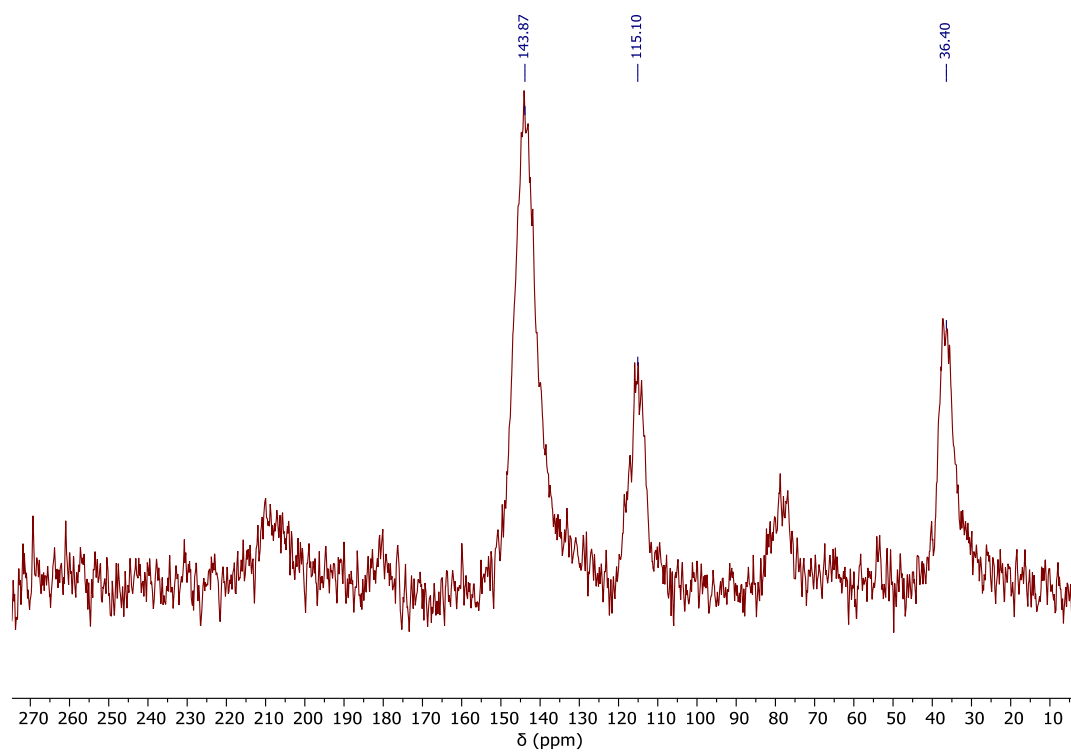


Figure S17. $^{13}\text{C}\{^1\text{H}\}$ NMR spectrum of solid L2.

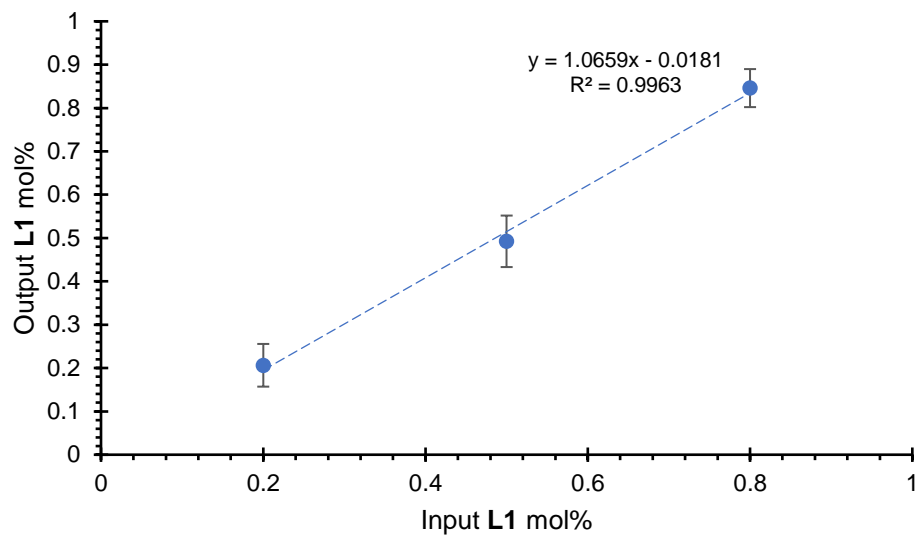


Figure S18. input-output plot of $[(L1)_x(L2)_{1-x}Cu_2Br_2]$ with output mol% determined via integration of the B and B' peaks of the $^{13}C\{^1H\}$ solid-state NMR spectra. Error bars were determined by analysis of the S/N ratio of each spectrum.

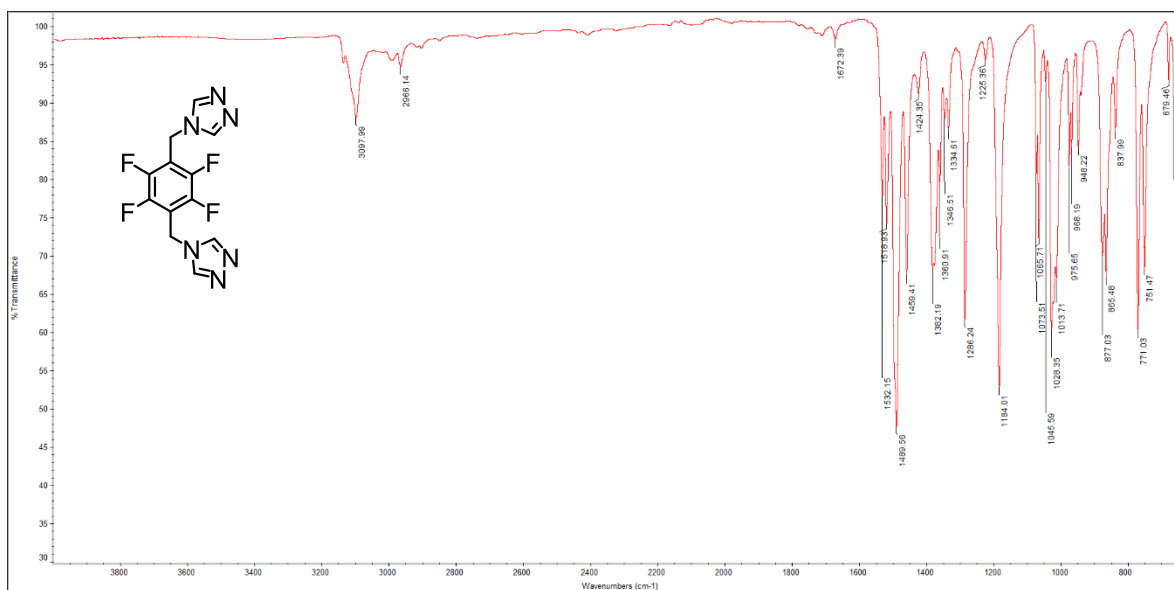


Figure S19. ATR-IR spectrum of L2.

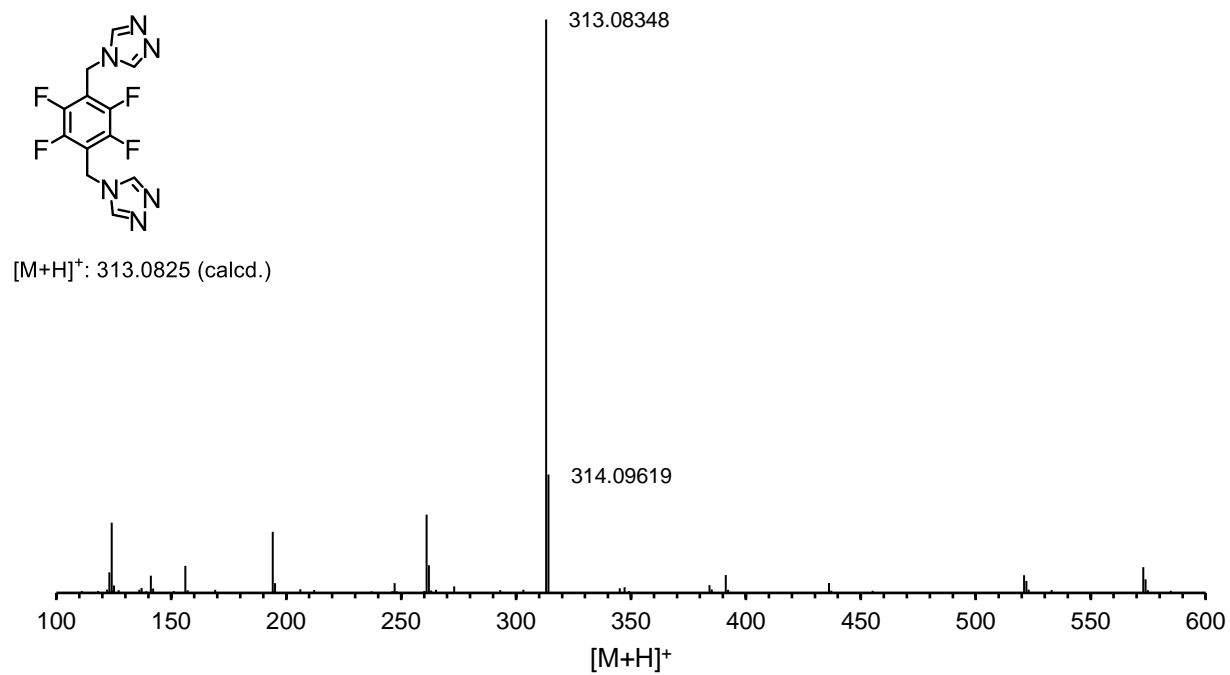


Figure S20. HR DART-MS of L2.

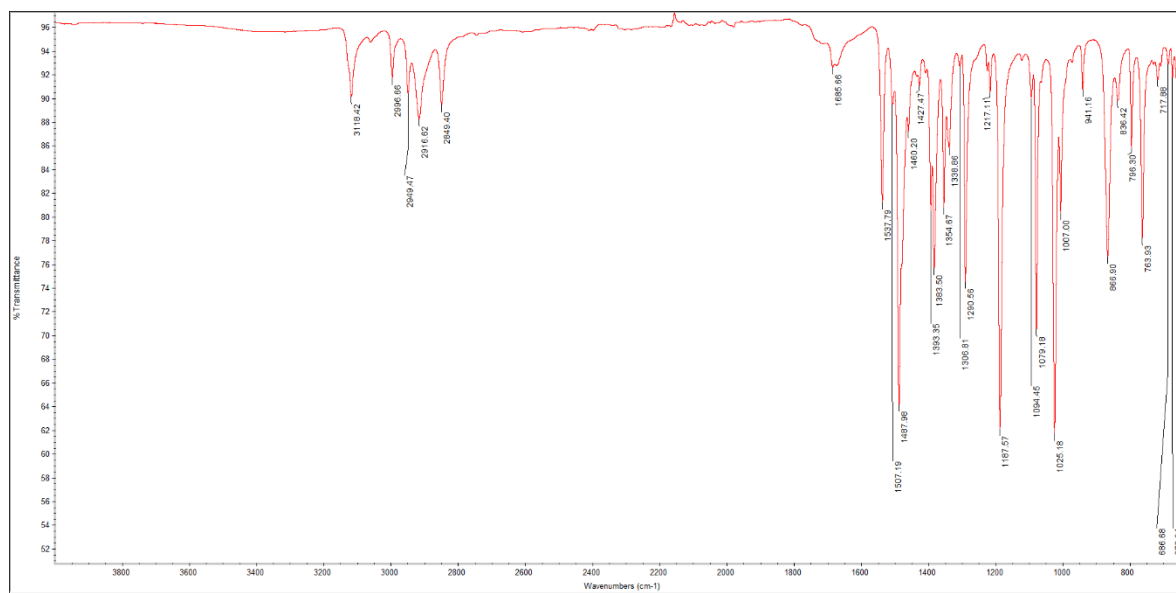


Figure S21. ATR-IR of $[(L2)Cu_2Br_2]$.

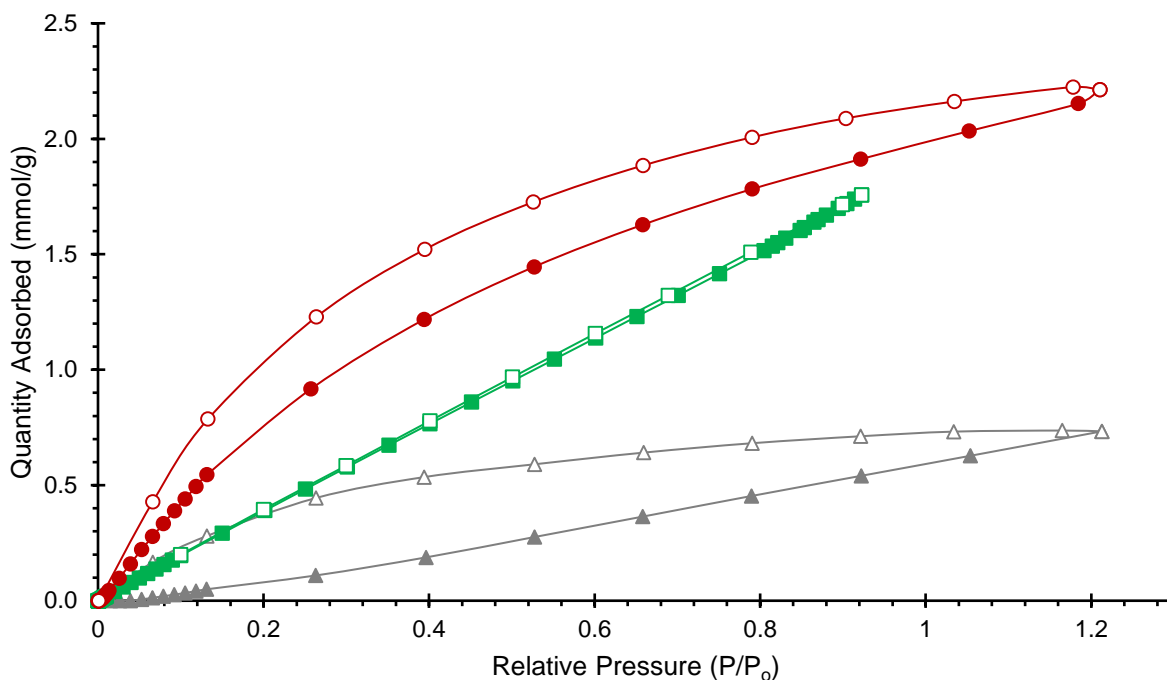


Figure S22. Volumetric adsorption isotherms of $[(L2)Cu_2Br_2]$ MONT. Red circles represent CO_2 , grey triangles represent CH_4 , and green squares represent H_2 . Filled symbols represent adsorption and empty symbols represent desorption, respectively.

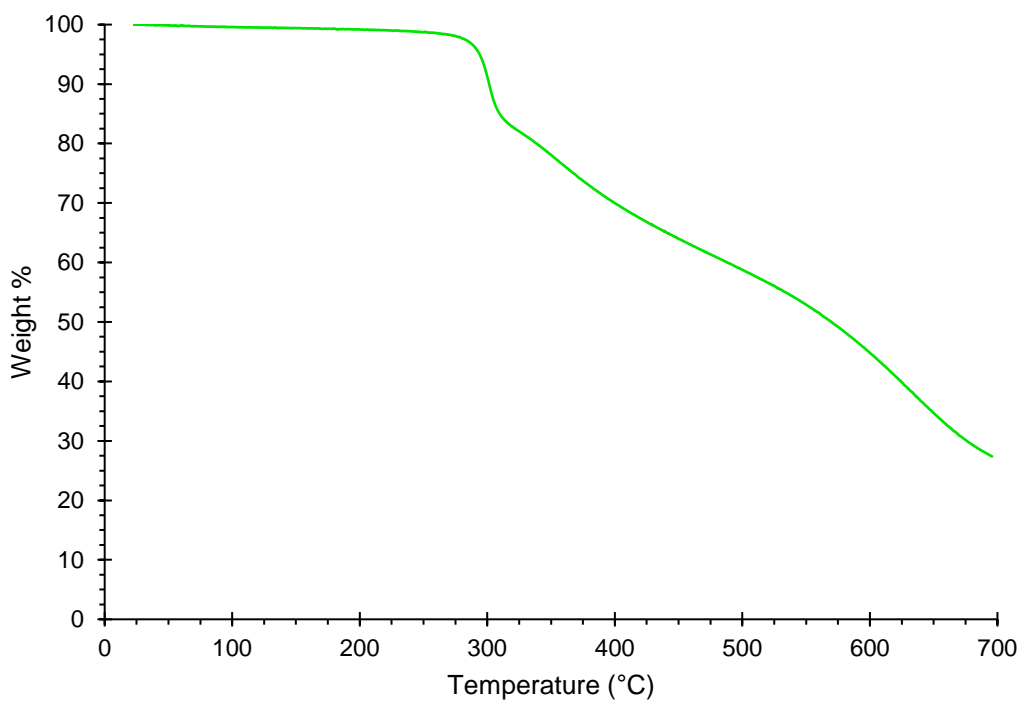


Figure S23. TGA for $[(L2)Cu_2Br_2]$.

IV. Powder X-ray Diffraction Data

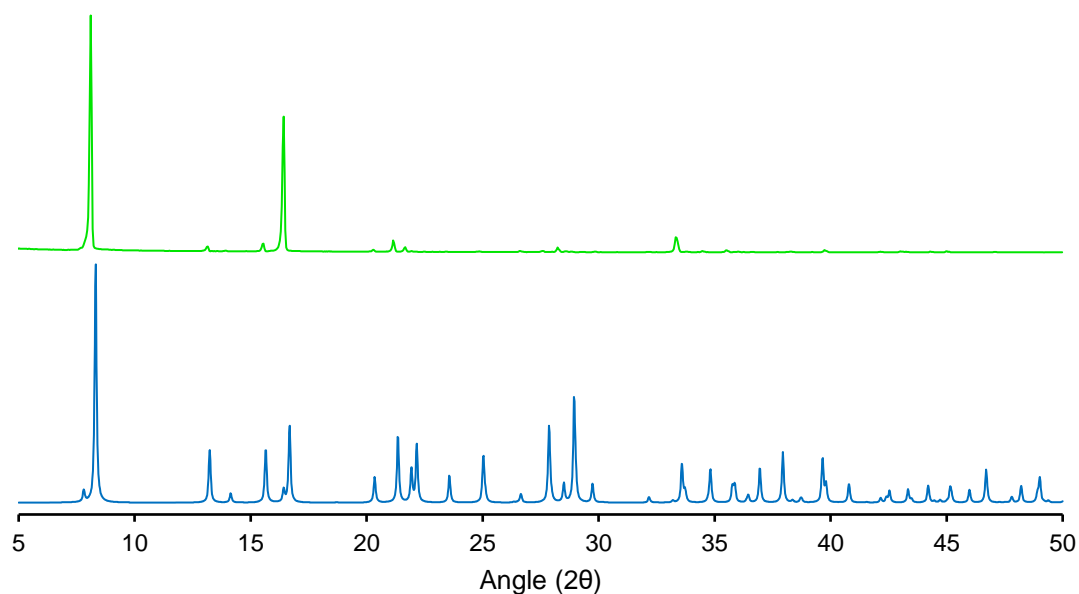


Figure S24. PXRD pattern for $[(L2)Cu_2Br_2]$: experimental (green, upper) and simulated (blue, lower).

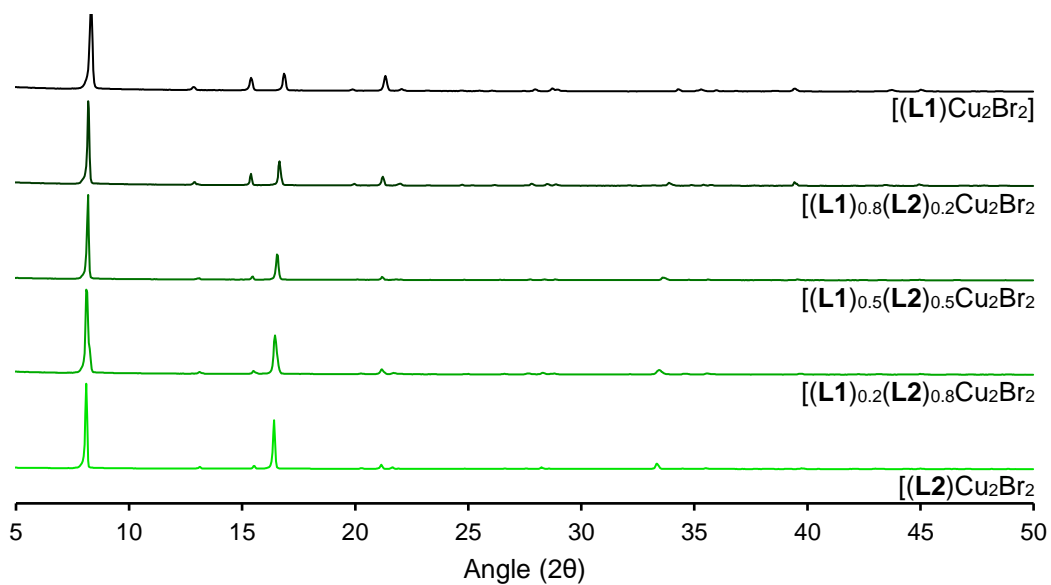


Figure S25. PXRD pattern of $[(L1)_x(L2)_{1-x}]Cu_2Br_2$ mixed-ligand MONTs (shown with $x = 1$ at top).

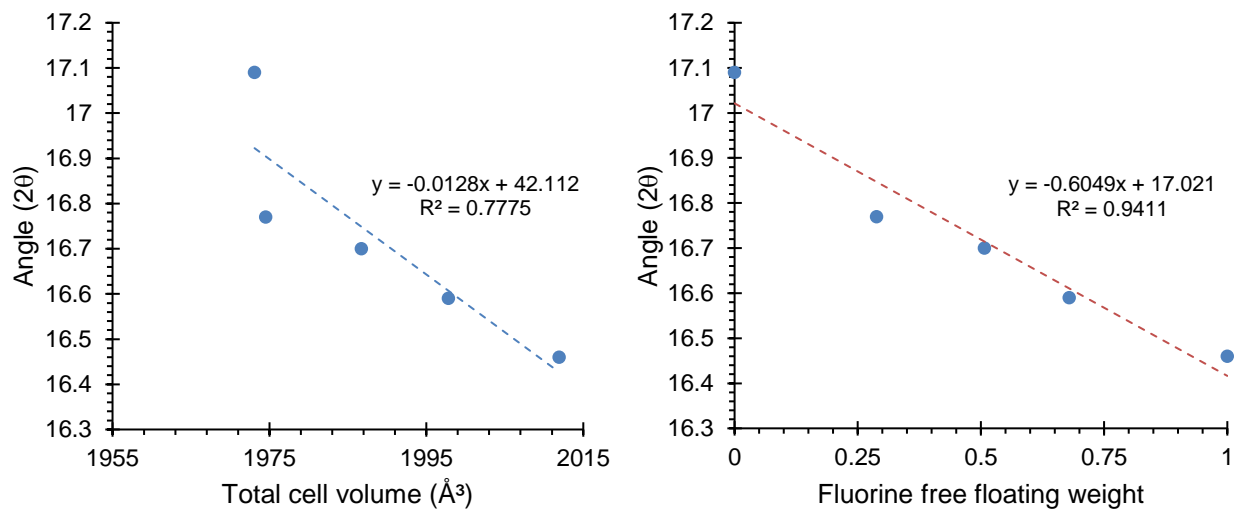


Figure S26. Peak positions of the $hkl = 400$ signals of $[(L1)_x(L2)_{1-x}Cu_2Br_2]$ plotted against the total cell volume (left) and the fluorine free floating weight (right).

V. Selected Area Electron Diffraction

TEM sample preparation:

Stock solutions of MONT precursor were made by dissolving 0.91 mg di-triazole ligand (**L1**) in 1 mL DMF, 1.18 mg fluorinated di-triazole ligand (**L2**) in 1 mL DMF, and 3.36 mg CuBr₂ in 1 mL water. MONTs were prepared with 5 different ligand compositions where the **L1** to **L2** ratio was altered: 1:0, 1:4, 1:1, 4:1, and 0:1, while maintaining the 1:2 CuBr₂ to organic linker ratio. Upon their preparation, MONT solutions were gently mixed and heated to 85 °C for 15 minutes. Following heating, the solutions were diluted by 10 times to better isolate individual MONT bundles for TEM. 9 μL of each diluted MONT solution were drop casted onto 300 mesh Lacey Carbon gold TEM grids purchased from Ted Pella Inc. After 30 seconds, the grids were then rinsed with distilled water to remove excess reactants and solvent. The grids were then placed on a single-tilt TEM holder for energy dispersive X-ray (EDX) spectroscopy and selected area electron diffraction (SAED). To determine how the fluorinated ligand was incorporated into the crystal structure, EDX was utilized to construct elemental maps of the MONTs. The use of EDX is crucial to confirm the random statistical of **L1** and **L2**.

TEM of bulk synthesized MONTs was performed using a JEOL 200CF operated at 200 kV. EDX and SAED were performed using a JEOL ARM200CF GrandARM TEM with a Gatan OneView-IS camera operated at 200 kV. SAED were acquired with spot size 5, selected area aperture 4, beam current of 15 μA, and exposure time of 0.5 seconds. The lattice parameters of each structure were determined by measuring the distance between diffraction spots using the linear profile tool in the Gatan Digital Micrograph software.

SAED was utilized to verify the lattice parameter of nanoscale MONT bundles and compared with the bulk MONT bundles by SC-XRD. The MONT bundles exhibit SAED spots corresponding to the following lattice parameters: $a \approx 22 \text{ \AA}$, $b \approx 7 \text{ \AA}$, and $c \approx 14 \text{ \AA}$, as dictated by the orientation of the crystal (**Figure S23**, **Table S2**).

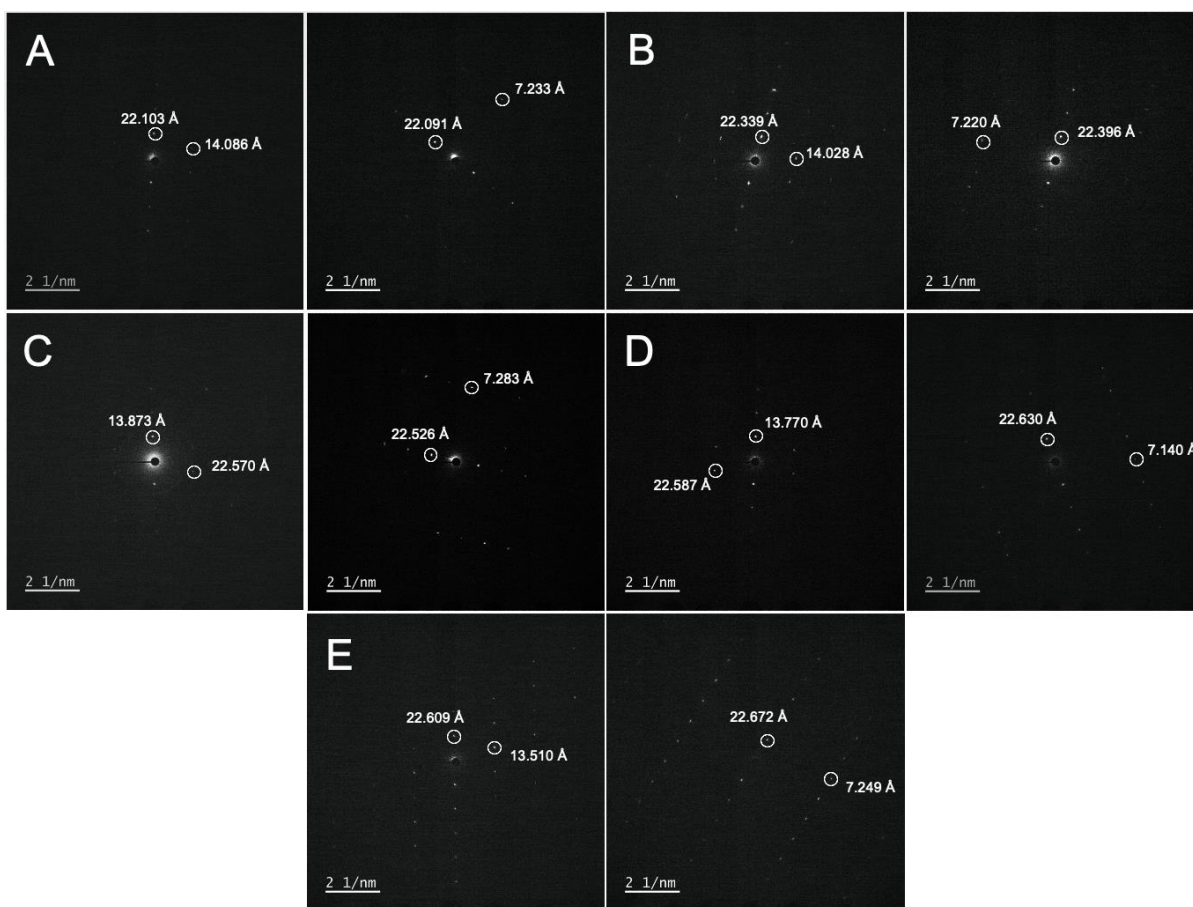


Figure S27. Verification of crystallinity. (A-E) SAED of MONT bundles corresponding to the crystal structures of $(\text{L1})\text{Cu}_2\text{Br}_2$, $(\text{L1})_{0.8}(\text{L2})_{0.2}\text{Cu}_2\text{Br}_2$, $(\text{L1})_{0.5}(\text{L2})_{0.5}\text{Cu}_2\text{Br}_2$, $(\text{L1})_{0.2}(\text{L2})_{0.8}\text{Cu}_2\text{Br}_2$, and $(\text{L2})\text{Cu}_2\text{Br}_2$ MONT bundles, respectively.

		$(\text{L1})\text{Cu}_2\text{Br}_2$	$(\text{L1})_{0.8}(\text{L2})_{0.2}\text{Cu}_2\text{Br}_2$	$(\text{L1})_{0.5}(\text{L2})_{0.5}\text{Cu}_2\text{Br}_2$	$(\text{L1})_{0.2}(\text{L2})_{0.8}\text{Cu}_2\text{Br}_2$	$(\text{L2})\text{Cu}_2\text{Br}_2$
SAED	a (Å)	22.097	22.368	22.548	22.609	22.641
Lattice	b (Å)	7.233	7.220	7.283	7.140	7.249
Parameter	c (Å)	14.086	14.028	13.873	13.770	13.510
SC-XRD	a (Å)	20.612	20.804	20.998	21.116	21.246
Lattice	b (Å)	7.029	7.017	7.031	7.051	7.083
Parameter	c (Å)	13.620	13.525	13.457	13.419	13.369

Table S2. Table including the lattice parameters for each MONT bundle determined by SAED.

The diffraction spots determined by SAED display the same trends as those measured by SC-XRD. In both techniques, we observed that lattice parameter a increases and lattice parameter c decreases upon increasing concentration of L2. Moreover, the lattice parameters measured by SAED and SC-XRD agree closely, with a difference of $< 2 \text{ \AA}$.

VI. STEM Imaging and Energy Dispersive X-ray Spectroscopy

EDX mapping was employed for elemental analysis of MONT grown in bulk. EDX elemental maps were acquired by probe size 8C, dwell time of 10 seconds, frame time of 20 seconds, beam current of 15 μ A, convergence semi-angle of 28 mrad, and a camera length of 6 cm. After data acquisition, the color maps were processed with a bin size of 5 kernels.

High-angle annular dark-field (HAADF) STEM images were obtained, which demonstrated that under the same synthesis conditions, the average size of the MONTs increased upon increasing the amount of fluorinated ligand (**Figure S24**, column 1). This suggests that the addition of fluorine may be responsible for increasing the kinetics of MONT formation. The EDX maps demonstrate a strong, uniform signal from Cu, Br, C, and N for each CuBr MONT bundle (**Figure S24**, columns 2,3,5,6). EDX mapping also shows a weak fluorine signal that becomes stronger when the composition of the organic linker is composed of over 20% of L2 (**Figure S24**, column 4). Due to the uniform signal coming from each MONT bundle, EDX data confirms that the MONT bundles consist of statistically co-polymerized ligands.

We note that the signal-to-noise ratio seems to decrease with increasing concentration of LC due to the increasing size of individual MONT bundles. The corresponding EDX spectra display sharp peaks for Cu, Br, N, and C (**Figure S25**). The EDX spectra also confirm a sharp increase in signal from F that corresponds to the increasing concentration of L2.

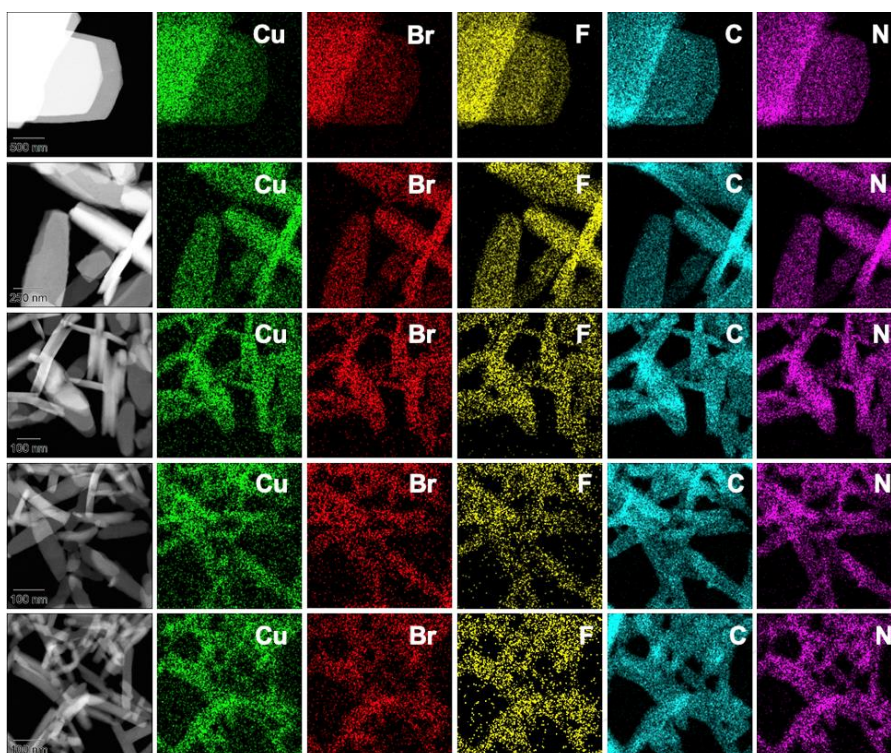


Figure S28. EDX analysis of MONT bundles grown at 85 °C. HAADF-STEM image and elemental maps confirming the formation of $(L1)Cu_2Br_2$, $(L1)_{0.8}(L2)_{0.2}Cu_2Br_2$, $(L1)_{0.5}(L2)_{0.5}Cu_2Br_2$, $(L1)_{0.2}(L2)_{0.8}Cu_2Br_2$, and $(L2)Cu_2Br_2$ MONT bundles.

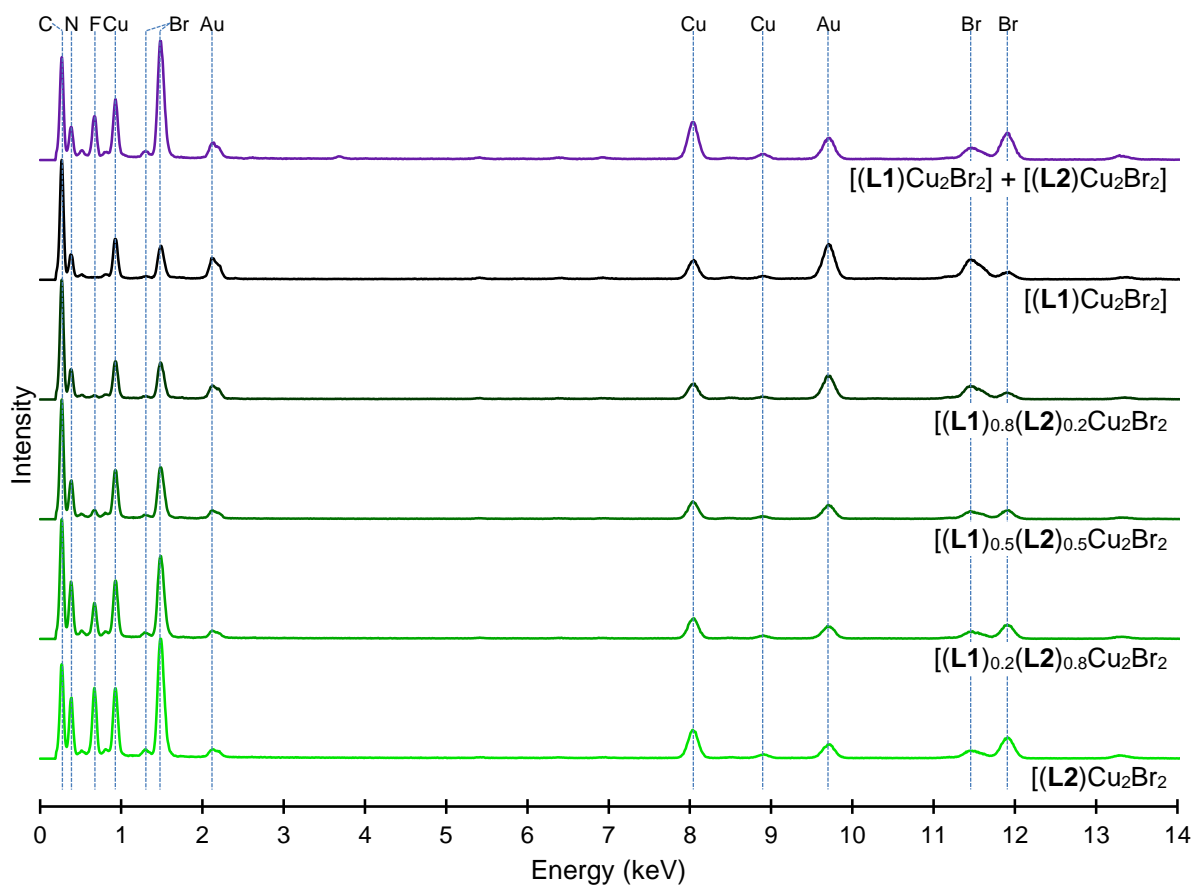


Figure S29: EDS spectra confirm the formation of $(\mathbf{L1})\text{Cu}_2\text{Br}_2$, $(\mathbf{L1})_{0.8}(\mathbf{L2})_{0.2}\text{Cu}_2\text{Br}_2$, $(\mathbf{L1})_{0.5}(\mathbf{L2})_{0.5}\text{Cu}_2\text{Br}_2$, $(\mathbf{L1})_{0.2}(\mathbf{L2})_{0.8}\text{Cu}_2\text{Br}_2$, and $(\mathbf{L2})\text{Cu}_2\text{Br}_2$. Purple represents a 50/50 mix of $(\mathbf{L1})\text{Cu}_2\text{Br}_2$ and $(\mathbf{L2})\text{Cu}_2\text{Br}_2$. MONT bundles with a noticeable increase in the intensity of the fluorene peak corresponding to the incorporation of $\mathbf{L2}$ into the MONT bundles. The gold signal is retained throughout each spectrum due to the signal resulting from the gold TEM grid.

VII. References

1. A. Horváth, *Synthesis*, 1995, **9**, 1183–1189.
2. C. R. Murdock, N. W. McNutt, D. J. Keffer and D. M. Jenkins, *J. Am. Chem. Soc.*, 2014, **136**, 671–678.
3. G. R. Fulmer, A. J. M. Miller, N. H. Sherden, H. E. Gottlieb, A. Nudelman, B. M. Stoltz, J. E. Bercaw and K. I. Goldberg, *Organometallics*, 2010, **29**, 2176–2179.
4. C. R. Morcombe and K. W. Zilm, *J. Magn. Reson.*, 2002, **162**, 479-486.
5. C. P. Rosenau, B. J. Jelier, A. D. Gossert and A. Togni, *Angew. Chem. Int. Ed.*, 2018, **57**, 9528–9533.
6. H. Okamoto, T. Kozai, Z. Okabayashi, T. Shinmyozu, H. Ota, K. Amimoto and K. Satake, *J. Phys. Org. Chem.*, 2017, **30**, e3726.